World Journal of Surgical Oncology

RESEARCH

Open Access

Inhibition of HOXC11 by artesunate induces ferroptosis and suppresses ovarian cancer progression through transcriptional regulation of the PROM2/PI3K/AKT pathway

Jun Li[1,2†], Lu Feng[2†], Yijun Yuan[2], Tianwen He[2], Xinru Zou[2], Bin Su[2], Kang Liu[3] and Xiaojun Yang[1*]

Abstract

Background Ferroptosis, a non-apoptotic form of regulated cell death, plays a critical role in the suppression of various tumor types, including ovarian cancer. Artesunate (ART), a derivative of artemisinin, exhibits extensive antitumor effects and is associated with ferroptosis. This study aimed to investigate the mechanisms through which ART induces ferroptosis to inhibit ovarian cancer.

Methods RNA sequencing was conducted to identify differentially expressed genes associated with ART-induced ferroptosis. Dual-luciferase reporter assays and electrophoretic mobility shift assays were performed to confirm the interaction between Homeobox C11 (HOXC11) and the Prominin 2 (PROM2) promoter. Cell Counting Kit-8 (CCK-8) assays, flow cytometry, and wound healing assays were used to analyze the antitumor effects of ART. Western blot, biochemical assays and transmission electron microscope were utilized to further characterize ART-induced ferroptosis. In vivo, the effects of ART on ferroptosis were examined using a xenograft mouse model.

Results RNA sequencing analysis revealed that the HOXC11, PROM2 and Phosphatidylinositol 3-Kinase/ Protein Kinase B (PI3K/AKT) pathways were downregulated by ART. HOXC11 was found to regulate PROM2 expression by binding to its promoter directly. HOXC11 overexpression reversed ART-induced effects on ovarian cancer cell proliferation, migration, apoptosis and ferroptosis by activating the PROM2/PI3K/AKT signaling axis. Conversely, silencing PROM2 in HOXC11-overexpressing cells restored ART-induced ferroptosis and its associated antitumor effects by inhibiting the PI3K/AKT pathway. Consistently, in vivo studies using a xenograft mouse model confirmed that ART-induced tumor inhibition was mediated by ferroptosis through the suppression of the HOXC11/PROM2/PI3K/AKT pathway.

Conclusion This study identifies the HOXC11/PROM2/PI3K/AKT axis as a novel regulatory mechanism underlying ART-induced ferroptosis in ovarian cancer. Targeting the HOXC11/PROM2 axis may represent a promising therapeutic strategy for enhancing ferroptosis, offering new insights for the treatment of ovarian cancer.

Keywords Artesunate, HOXC11, PROM2, Ferroptosis, PI3K/AKT signaling, Ovarian cancer

† Jun Li and Lu Feng contributed equally to this work.

*Correspondence:
Xiaojun Yang
yang.xiaojun@hotmail.com
Full list of author information is available at the end of the article

Introduction

Ovarian cancer is a major cause of morbidity and mortality among women worldwide [1]. With an incidence of 3.4% and a mortality of 4.7%, ovarian cancer has become the eighth most common and the fifth deadliest malignant tumor, posing a significant threat to the health of women [2, 3]. Therefore, it is urgent to elucidate the mechanisms underlying the development and progression of ovarian cancer and to identify novel therapeutic targets for the treatment of ovarian cancer [1, 4].

Ferroptosis, first identified in 2012, is a form of regulated cell death distinct from apoptosis, necrosis, and autophagy. It is characterized by the accumulation of iron-dependent lipid peroxides, leading to cell death [5]. Emerging evidence suggests that ferroptosis plays a crucial role in various diseases, including cancer [6–8]. Glutathione peroxidase 4 (GPX4), a key regulator of ferroptosis, has attracted attention as a potential therapeutic target in cancer treatment. Inhibiting GPX4 activity has been shown to enhance ferroptosis and sensitize tumors to treatment [9, 10]. Additionally, the Phosphatidylinositol 3-Kinase/Protein Kinase B (PI3K/AKT) signaling pathway has been implicated in ferroptosis regulation. Several inducers, such as curcumin, promote ferroptosis by inhibiting the PI3K/AKT/mTOR (Mammalian Target of Rapamycin) pathway, thereby suppressing cancer cell proliferation in gastric cancers [11]. Similarly, Krüppel-like factor 2 (KLF2) induces ferroptosis by inhibiting PI3K/AKT signaling, reducing colorectal cancer cell migration and invasion [12]. In ovarian cancer, it has been shown that inducing ferroptosis in combination with chemotherapy can significantly enhance therapeutic efficacy, particularly in platinum-resistant tumors [13]. Furthermore, the degradation of p53 has been linked to ferroptosis suppression and increased tumorigenesis in ovarian cancer [14]. These findings suggest that the potential of targeting ferroptosis as a promising therapeutic strategy for ovarian cancer.

Transcription factors, which are pivotal regulators of gene expression, play essential roles in cancer progression and resistance. Among them, Homeobox C11 (HOXC11), a member of the HOX gene family, has garnered attention for its involvement in the tumorigenesis of several cancers, including colon, gastric, and lung adenocarcinomas [15–17]. However, the role of HOXC11 in ferroptosis and ovarian cancer progression has been poorly reported. Prominin 2 (PROM2) is a transmembrane glycoprotein and it has been implicated in cancer progression and ferroptosis resistance in several cancer types [18–20]. Nevertheless, the biological function of PROM2 in ovarian cancer is still unclear. These knowledge gaps present opportunities for further research into the role of the HOXC11/PROM2 axis in ovarian cancer pathogenesis and therapy.

Artesunate (ART), a derivative of artemisinin originally developed for its antimalarial properties, has gained significant attention for its potent anticancer effects [21, 22]. ART induces ferroptosis by increasing intracellular iron levels and promoting ROS production, leading to oxidative damage and cell death in several types of cancer, including ovarian cancer [23–25]. Our previous research revealed that ART drives ferroptosis in ovarian cancer cells [26]. However, the mechanism of ART-induced ferroptosis-mediated tumor suppression in ovarian cancer remains unclear.

In the present study, we aimed to evaluate the mechanism of ferroptosis-mediated tumor suppression induced by ART in ovarian cancer. We focus on the role of HOXC11, which we hypothesize to act as a key transcriptional regulator of the PROM2/PI3K/AKT pathway, a critical axis involved in ferroptosis resistance and cancer progression. By elucidating the HOXC11/PROM2 axis, we seek to uncover novel therapeutic targets that could help overcome treatment resistance in ovarian cancer. Our findings may provide valuable insights into the development of ferroptosis-based therapies, offering new potential target for improved ovarian cancer treatments in the future.

Materials and methods

Cell culture

The human ovarian cancer cell lines SKOV3 and ES2 were purchased from the National Collection of Authenticated Cell Cultures (Shanghai, China). SKOV3 and ES2 cells were cultured in McCoy's 5a medium (Gibco, 16600082) supplemented with 10% fetal bovine serum (FBS, Gibco, 10091155), 100 U/ml penicillin and 100 μg/ml streptomycin (HyClone, SV30010). The culture condition was 37 °C and a humidified atmosphere with 5% CO2. The cells were subcultured every 2–4 days according to cell confluence.

RNA sequencing (RNA-seq) analysis

ES2 cells were treated with 40 μM ART (MCE, HY-N0193) or DMSO (vehicle control) for 24 h. Total RNA was extracted using TRIzol reagent (Invitrogen, c#15596026). RNA quality was tested by examining the A260/A280 ratio with NanoDrop (Thermo Fisher Scientific, USA). RNA-seq libraries were constructed using the Invitrogen Collibri Stranded RNA Library Prep Kit (Invitrogen Life Technologies, A39117024) according to the manufacturer's instructions. Paired-end sequencing was performed on an Illumina HiSeq 4000 platform (Illumina, USA). Differentially expressed genes (DEGs) between the control and ART treatment groups were

analyzed using the DESeq2 R package. Significant differences in gene expression were determined according to the criteria of $|\log_2 FC| > 1$ and p value < 0.01. Functional annotation and enrichment analysis were performed using the Gene Ontology (GO) database (http://www.geneontology.org/) and the Kyoto Encyclopedia of Genes and Genomes (KEGG) Mapper (http://www.genome.jp/kegg/mapper.html), respectively. The clusterProfiler R package was used for enrichment analysis.

Quantitative real-time polymerase chain reaction (qRT–PCR) analysis

Total RNA was extracted from cells using TRIzol reagent (Yeasen, 10606ES60). RNA concentration and purity were checked with NanoDrop. cDNA was synthesized using the HiScript IV 1st Strand cDNA Synthesis Kit (Vazyme, R412-01) according to the manufacturer's protocol. qRT-PCR was performed with QuantStudio 12 K (Thermo Fisher Scientific, USA) using Hieff® qPCR SYBR Green Master Mix (Low Rox) (Yeasen, 11202ES08). The PCR program was as follows: denaturation at 95 °C for 5 min, followed by 40 cycles of 95 °C for 10 s, 60 °C for 20 s and 72 °C for 20 s. GAPDH was used as an internal control, and the data were analyzed using the $2^{-\Delta\Delta ct}$ method. The primers used for amplification were listed in Table 1.

Western blot analysis

Cells or tissues from each experimental group were harvested and washed with PBS. Total protein was extracted with RIPA Lysis Buffer (Beyotime, P0013) containing protease and phosphatase inhibitor cocktail (Beyotime, P1045). Protein concentration was detected using a BCA assay kit (Beyotime, P0012). Equal amounts of protein (30 μg per sample) were separated by SDS-PAGE and transferred to an NC membrane. Membrane was blocked with 5% nonfat milk and then incubated with primary antibody at 4 °C overnight. The dilution ratios for primary antibodies were as follows: GAPDH (Proteintech, 10494-1-AP) at 1:10000; Bax (Proteintech, 50599-2-Ig), GPX4 (Proteintech, 67763-1-Ig), and Bcl-2 (Proteintech, 12789-1-AP) at 1:5000; AKT (Proteintech, 60203-2-Ig), p-AKT (Proteintech, 66444-1-Ig), and PIK3CG (Abcam, ab140307) at 1:2000; HOXC11 (Novus Biologicals, OTI3E10), PROM2 (Affinity, DF14670), and p-PI3K (CST, 17366) at 1:1000. The dilutions of the goat anti-rabbit and goat anti-mouse secondary antibodies were 1:5000. Proteins were visualized using BeyoECL Plus (Beyotime, P0018S), and detected with a ChemiDoc™ XRS + system (Bio-Rad, USA). Relative protein levels were measured by ImageJ (Rasband, USA) and normalized to GAPDH.

Table 1 Primer sequences for qRT-PCR

Primer name	Sequence (5'-3')
PROM2-F	CATCAGCATCCACCAAGCCTATC
PROM2-R	TGCAACTCCTGCCGTAGCTTGT
HOXC11-F	GCACCATCGGAACAGCTACT
HOXC11-R	GATCTCGGTGACGGTGGAAG
PIK3CG-F	CCTTCACAGAGGAGGTGCTG
PIK3CG-R	ACCGCAGTAGATCTGGAGGT
GAPDH-F	TCAAGAAGGTGGTGAAGCAGG
GAPDH-R	TCAAAGGTGGAGGAGTGGGT

Dual-luciferase reporter assay

The coding sequence (CDS) of HOXC11 was inserted into the pcDNA3.1 plasmid, and the promoter sequence of PROM2 was inserted into the upstream of a luciferase reporter gene in the pGL3-basic plasmid. pcDNA3.1-HOXC11 and pGL3-PROM2 were co-transfected with pRL-TK into HEK-293T cells using Lipofectamine 2000 (Invitrogen, 11668019) according to the manufacturers' protocols. The empty pcDNA3.1 and pGL3-basic vectors were used as controls. After 48 h of transfection, cells were lysed, and a Dual-Luciferase Reporter Assay System (Promega, E1910) was used for the luciferase activity assay according to the manufacturers' protocols. Relative luciferase activity was calculated as the ratio of firefly to Renilla luciferase activity.

Electrophoretic mobility shift assay (EMSA)

The full-length sequence of HOXC11 was inserted into the pET-28b vector and transformed into *Escherichia coli* BL21 (DE3). Isopropyl β-d-1-thiogalactopyranoside (IPTG, 1 mM) was used to induce recombined protein at 37°C for 5 h. The recombinant HOXC11 protein was purified using Ni-NTA-agarose resin (Qiagen). DNA probes were labeled with biotin at the 3' end using an EMSA Probe Biotin Labeling Kit (Beyotime, GS008). The EMSA was carried out using a LightShift Chemiluminescent EMSA Kit (Thermo Fisher, 20148) following the instruction.

Recombinant lentivirus particles and cell line transduction

Recombinant lentivirus particles were obtained from GenePharma (Shanghai, China). ES2 and SKOV3 cells were transduced with lentivirus (MOI = 10) and 8 μg/ml polybrene for 2–3 days, followed by 2 μg/ml puromycin treatment until puromycin-resistant cells predominated. The overexpression of HOXC11 and knockdown efficiency of PROM2 were verified by western blot analysis.

CCK-8 assay

ES-2 and SKOV-3 cells were seeded in 96-well plates at a density of 9000 cells per well overnight. Cells were treated with 40 μM ART for 24 h. Cell viability was measured using the Cell Counting Kit-8 reagent (Dojindo, CK04).

Flow cytometry analysis

ES-2 and SKOV-3 cells were seeded in 24-well plates at a density of 8×10^4 cells per well overnight. An Annexin V-FITC Apoptosis Detection Kit (Beyotime, C1062M) was used according to the manufacturer's instructions for the apoptosis assay. Briefly, cells were suspended in 200 μL of Annexin binding buffer containing 5 μL of Annexin V-FITC and 10 μL of propidium iodide (PI). After incubating in the dark at room temperature for 10–20 min, cell apoptosis was tested by flow cytometry (Agilent, USA). Lipid peroxides were tested using BODIPY 581/591 C11 (Invitrogen, D3861) staining. Cells were incubated with 5 μM BODIPY for 30 min at 37℃and analyzed by flow cytometry.

Wound healing assay

ES-2 and SKOV-3 cells were seeded in 6-well plates at a density of 6×10^5 cells per well overnight. When cell confluence exceeded 90%, a 10 μL pipette tip was used to make a scratch in the bottom of the plates. Cells were washed with PBS and incubated in serum-free medium. Images of wound healing were taken by microscope (Olympus, Japan) at 0 h, 24 h and 48 h post-scratch.

Reactive oxygen species (ROS) detection

ROS assay was performed using ROS Assay Kit (Beyotime, S0033S). Cells were incubated with 10 μM DCFH-DA at 37 °C for 20 min. The cells were washed with serum-free medium for 3 times, and images of green fluorescence intensity were tested by microscope.

Biochemical index detection

Cells or tissues from the indicated groups were collected. Superoxide dismutase (SOD) activity, glutathione (GSH) concentration, and malondialdehyde (MDA) concentration were examined using a SOD activity assay kit (Nanjing Jiancheng Bioengineering Institute, A001-3), a GSH assay kit (Nanjing Jiancheng Bioengineering Institute, A006-2-1) and an MDA assay kit (Beyotime, S0131S), respectively, according to the manufacturer's guidelines.

Transmission electron microscope (TEM) analysis

ES-2 and SKOV-3 cells were fixed in 2.5% glutaraldehyde solution at room temperature for 2 h. Then, the cells were dehydrated and embedded in resin. Ultrathin sections were stained with uranyl acetate and lead citrate. The cell ultrastructure was observed under a transmission electron microscope (Hitachi H-7650, Japan).

Xenograft mouse model

5–6 weeks old female BALB/c nude mice were purchased from SiPeiFu (Beijing) Biotechnology Co., Ltd. A total of 5×10^6 SKOV3 cells were injected subcutaneously into the right flank of the mice to establish a xenograft model. Mice with approximately 100 mm^3 SKOV3 tumor xenografts were randomly divided into two groups ($n=6$ per group). Mice were intraperitoneally injected with vehicle (5% DMSO + 95% PBS) or 70 mg/kg ART for 25 days. Tumor volume and body weight were measured every three days. Tumor volume was calculated using the following formula: volume (mm^3) = 1/2 × (tumor length) × (tumor width)^2, length > width. Mice were euthanized at the end of the treatment period, and tumor tissues were collected for further analysis. All animal experiments were performed under the institutional guidelines and were approved by the Ethics Committees of North Sichuan Medical College (NSMC2023 (114)).

Immunohistochemistry (IHC) assay

Tumor tissues were fixed in 4% paraformaldehyde, embedded in paraffin, and cut into 5 μm slices. The slides were deparaffinized and rehydrated. After incubating with methanol containing 3% H_2O_2 and heat-inducing antigen retrieval by boiling in sodium citrate, the slides were blocked with goat serum for 30 min and incubated with primary antibodies at 4 °C overnight. The primary antibodies used were against GPX4 (1:1000, Proteintech, 67763-1-Ig), HOXC11 (1:100, Novus Biologicals, OTI3E10), and PROM2 (1:100, Affinity, DF14670). After incubation with a secondary antibody, proteins of interest were visualized with DAB solution (Beyotime, P0202), and the nuclei were stained with hematoxylin (Beyotime, C0107). Images were taken using a microscope (Olympus, Japan).

Statistical analysis

All data were analyzed using GraphPad Prism 8.0.2. The data were shown as mean ± standard deviation (SD). Two-tailed Student's t test was used for comparisons between two independent groups, and one-way ANOVA was used for comparisons multiple independent groups. $P<0.05$ was considered to indicate statistical significance.

Results

Identification of ferroptosis-related genes induced by ART in ovarian cancer cells

Our previous research revealed that ART induces ferroptosis in ovarian cancer cells [26]. To further investigate the underlying mechanisms of ART-induced ferroptosis,

RNA-seq was performed on ES2 cells. ES2 cells were treated with either 40 μM ART or DMSO for 24 h. As shown in Fig. 1A, a total of 879 significant DEGs were identified, including 192 upregulated and 687 downregulated genes. Moreover, KEGG pathway enrichment analysis revealed that downregulated DEGs were significantly enriched in the PI3K-AKT signaling pathway, which is associated with ferroptosis suppression (Fig. 1B). To further explore ferroptosis suppressors, 229 ferroptosis suppressor genes were obtained from the FerrDb database (http://www.zhounan.org/ferrdb/current/), and 9 candidate genes were identified by overlapping data from the FerrDb database with downregulated DEGs in the ART-treated groups (Fig. 1C). Among them, PROM2 has been reported to be associated with ferroptosis and to regulate the AKT pathway. However, there are few research reports on PROM2 in ovarian cancer, leading us to select PROM2 as a candidate for further study. Subsequently, we predicted the upstream transcription factors of the PROM2 promoter using the online tools UCSC (http://genome.ucsc.edu/) and AnimalTFDB (http://bioinfo.life.hust.edu.cn/AnimalTFDB/#!/). After overlapping predicted transcription factors with DEGs positively correlated with PROM2 expression, HOXC11 emerged as a potential transcription factor regulating the expression of PROM2 (Fig. 1D). The heatmap showed that the expression profiles of HOXC11, PROM2 and DEGs enriched in the PI3K/AKT pathway were positively correlated, all of which were decreased in the ART-treated groups (Fig. 1E).

To validate the DEGs identified by RNA-seq, ES2 and SKOV3 cells were treated with ART or DMSO, followed by qRT-PCR and western blot analyses. The qRT-PCR results indicated that HOXC11, PROM2 and PIK3CG expression was significantly downregulated in the ART-treated group. (Vehicle vs. ART, $p < 0.05$) (Fig. 1F). Similarly, the western blot results were consistent with the qRT-PCR findings, with protein levels of HOXC11, PROM2 and PIK3CG reduced in the ART-treated group (Fig. 1G, H). These results confirm the reliability of DEGs identified by RNA-seq. Taken together, these results indicated that the HOXC11, PROM2 and PI3K/AKT pathways could be involved in ART-induced ferroptosis in ovarian cancer cells.

HOXC11 regulated PROM2 expression by binding to the PROM2 promoter directly

The transcription binding site of HOXC11 in the PROM2 promoter was further predicted using JASPAR (http://jaspar.genereg.net/). The PROM2 promoter region at -303 to -292 bp relative to the transcription start site was identified as a putative HOXC11 binding site (Fig. 2A, D). The prediction was confirmed by a dual-luciferase reporter assay. The results showed that luciferase activity driven by the PROM2 promoter significantly increased in the presence of the HOXC11 overexpression vector (Fig. 2B). To further confirm this, purified recombinant HOXC11 protein expressed in *E. coli* was used for the EMSA (Fig. 2C). As shown in Fig. 2E, a DNA-protein complex formed when the biotin-labeled PROM2 probe was incubated with recombinant HOXC11 protein, whereas preincubation with 100-fold or 200-fold cold probe decreased the binding activity. A competition assay demonstrated that the HOXC11 protein binds specifically to the binding site of the PROM2 promoter. For further validation, we established the HOXC11 overexpression cell lines ES2 and SKOV3. As expected, the expression of PROM2 was significantly increased in HOXC11 overexpression cells when compared with empty vector (Fig. 2F). In brief, our data indicate that HOXC11 promotes PROM2 transcription by directly binding to the PROM2 promoter region.

HOXC11 overexpression suppressed the effects of ART on proliferation, apoptosis and migration in ovarian cancer cells

The involvement of HOXC11 in ART-induced tumor inhibition was investigated. First, we analyzed the viability of ES2 and SKOV3 cells using a CCK-8 assay. Compared with those in the control group, the survival rates of both ES2 and SKOV3 cells in the ART-treated group were significantly lower (ES2: 100% vs. 66.67%; SKOV3 100% vs. 61.28%, $p < 0.001$). However, overexpression of HOXC11 blocked the inhibition of proliferation induced by ART, and the survival rate was partially restored (ART + Vector vs. ART + HOXC11, $p < 0.01$) (Fig. 3A). Subsequently, flow cytometry results showed that ART strongly induced apoptosis in ES2 and SKOV3 cells, whereas HOXC11 overexpression attenuated ART-induced apoptosis (Fig. 3B). In addition, western blot analysis revealed that the apoptosis-related protein Bcl-2 was downregulated, while Bax was upregulated in the presence of ART. However, HOXC11 overexpression partially reversed the changes in the expression of these proteins (Fig. 3C, D). Moreover, cell migration ability was determined by wound healing assay. The cell migration rate of ES2 and SKOV3 cells was significantly reduced by ART. However, HOXC11 overexpression weakened the effect of ART and partially restored the migration ability of the ES2 and SKOV3 cells (Fig. 3E). Furthermore, based on the above results, we comprehensively analyzed the transcriptional regulatory mechanisms of HOXC11 involved in ART treatment. We evaluated the expression correlations between HOXC11 and the PROM2/PI3K/AKT axis in the presence of ART. Western blot results showed that the expression of HOXC11 and the PROM2/PI3K/AKT were inhibited by ART in both ES2

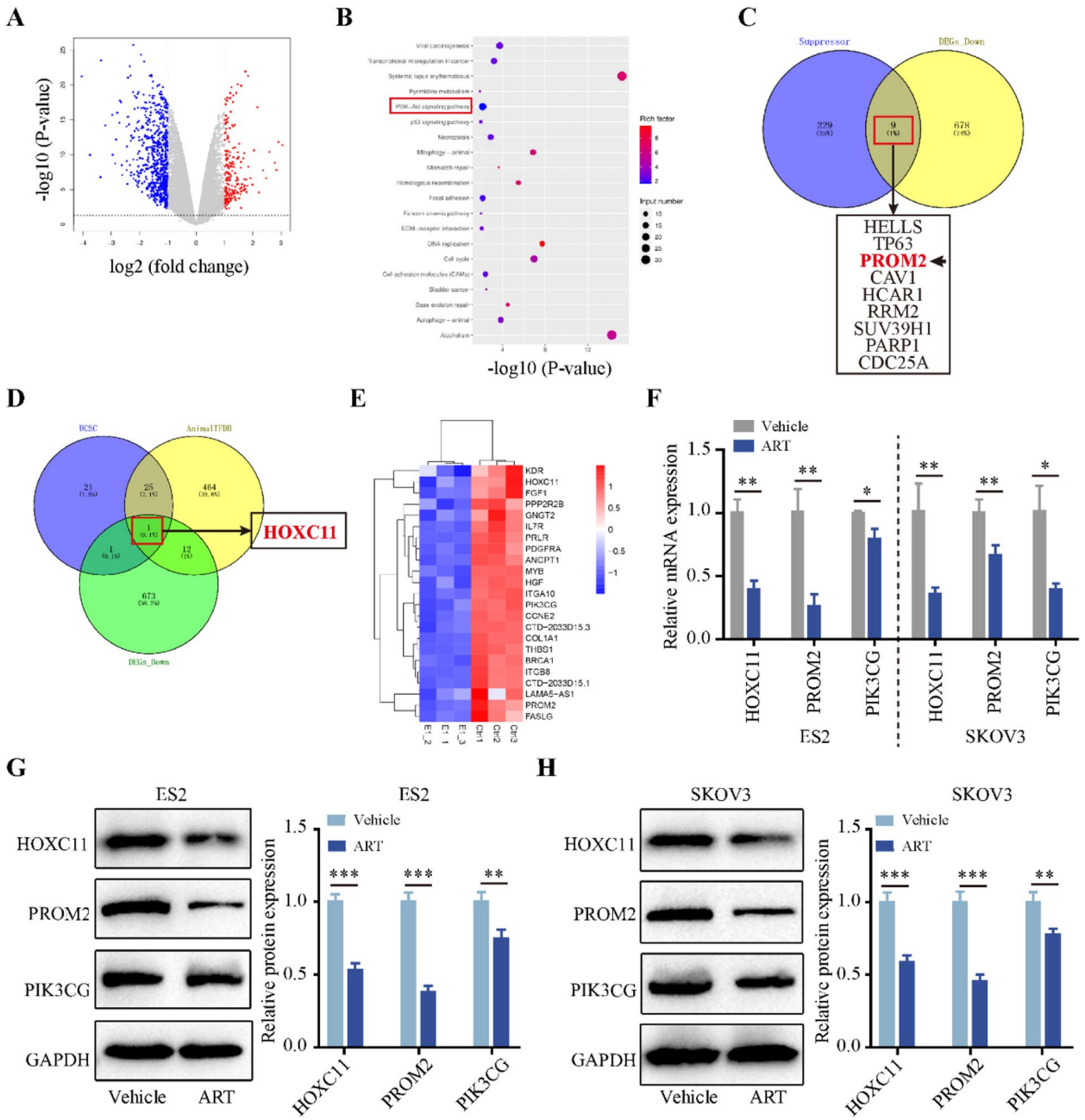

Fig. 1 Identification of ferroptosis-related genes induced by artesunate (ART) by RNA-seq (**A**) Volcano plot showed differentially expressed genes (DEGs) between control and ART-treated ES2 cells ($|\log_2 FC| > 1$ and p value < 0.01). The red dots represented upregulated genes, and the blue dots represented downregulated genes. The gray dots represented the genes expressed without significant changes. **B** The top 20 significantly enriched KEGG pathways for DEGs downregulated in the ART-treated groups; the PI3K-AKT signaling pathway is highlighted with a red rectangle. **C** Venn diagram showed the overlap between ferroptosis suppressor genes based on the FerrDb database (http://www.zhounan.org/ferrdb/current/) and downregulated DEGs in ART-treated ES2 cells according to RNA-seq. Nine candidate DEGs were identified, and PROM2 was chosen for further study. **D** Venn Diagram showed the overlaps of upstream transcription factors of the *PROM2* promoter predicted by UCSC (http://genome.ucsc.edu/) and AnimalTFDB (http://bioinfo.life.hust.edu.cn/AnimalTFDB/#!/), along with DEGs positively associated with *PROM2* expression according to RNA-seq. HOXC11 was identified as a candidate transcription factor. **E** Heatmap showed the expression of *HOXC11*, *PROM2*, and DEGs enriched in the PI3K-AKT signaling pathway. E1-E3 represented ART-treated ES2 cells, and Ctrl1-Ctrl3 represented control ES2 cells. **F** qRT–PCR analysis of *HOXC11*, *PROM2* and *PIK3CG* in ES2 and SKOV3 cells treated with DMSO (vehicle) or 40 μM ART for 24 h. Western blot analysis of HOXC11, PROM2 and PIK3CG in ES2 cells **G** and SKOV3 cells (H) treated with DMSO (vehicle) or 40 μM ART for 24 h. GAPDH was used as a loading control. The data were presented as relative expression levels and were analyzed as the mean ± SD of three independent experiments. *$p < 0.05$. **$p < 0.01$, ***$p < 0.001$

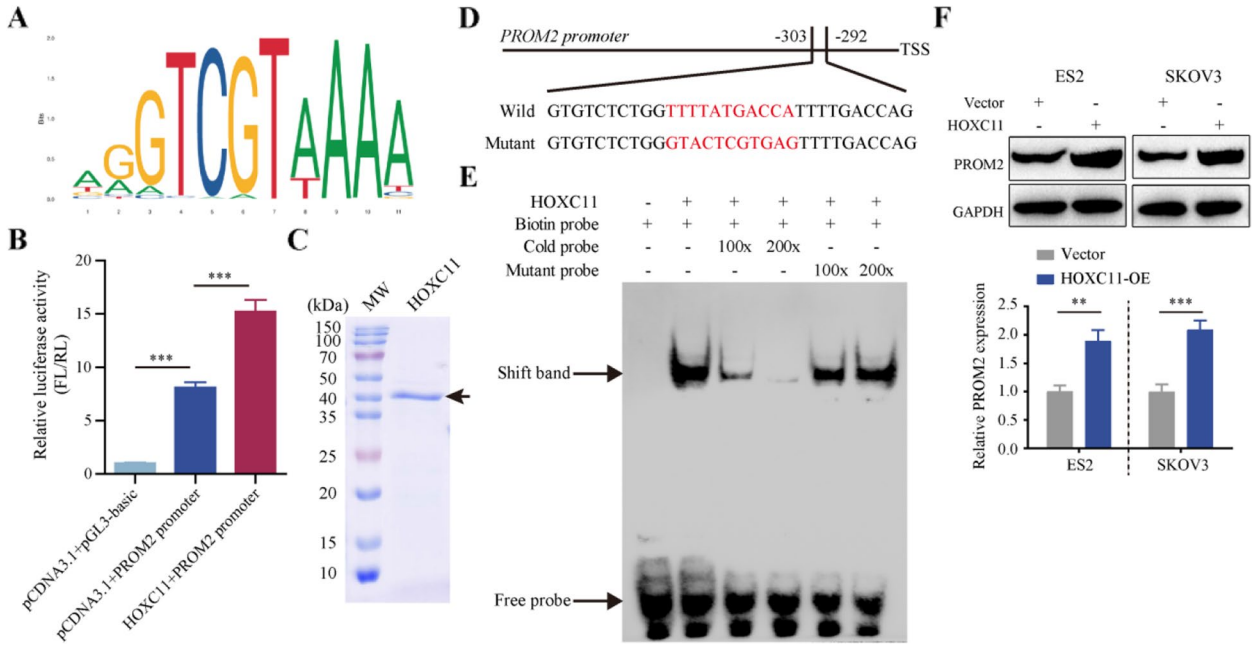

Fig. 2 The expression of PROM2 was regulated by HOXC11-mediated direct promoter region binding (**A**) The binding motif of HOXC11 was obtained from JASPAR (http://jaspar.genereg.net/). **B** Dual-luciferase reporter assay was used to determine the effect of HOXC11 overexpression on reporters containing PROM2 promoter sequences. Data were shown as the mean ± SD of three independent experiments. ***$p < 0.001$. **C** 2 μg of purified recombinant HOXC11 protein was analyzed by SDS–PAGE gel and stained with Coomassie brilliant blue. **D** The probe sequence used for the electrophoretic mobility shift assay (EMSA) of the promoter of PROM2. The core sequence for HOXC11 binding was highlighted in red. **E** EMSA revealed direct binding between the recombinant HOXC11 protein and biotin-labeled probes. Cold probe (unlabeled) and mutant probe were used as competitors. **F** Western blot analysis of PROM2 in control and HOXC11 overexpression ES2 (left) and SKOV3 cells (right). GAPDH was used as a loading control

and SKOV3 cells, while overexpression of HOXC11 activated the expression of PROM2/PI3K/AKT, which alleviated the inhibitory effect of ART. Since ART has been reported to induce ferroptosis in ovarian cancer cells, we also assessed the expression of GPX4, a ferroptosis marker. Interestingly, GPX4 was strongly inhibited by ART treatment, while the expression of GPX4 was restored by HOXC11 overexpression in the presence of ART (Fig. 3F, G). Collectively, HOXC11 overexpression suppressed ART-induced tumor inhibition in ovarian cancer cells by upregulating the PROM2/PI3K/AKT pathway and was involved in ART-induced ferroptosis.

HOXC11 enhanced ART-induced ferroptosis resistance in ovarian cancer cells

Next, we investigated the role of HOXC11 in ART-induced ferroptosis in ovarian cancer. Lipid peroxidations, ROS accumulation and GSH depletion are always accompanied by ferroptosis. Mitochondrial morphological abnormalities are characteristic of ferroptosis. We further detected the effect of HOXC11 on the levels of lipid peroxides, ROS, GSH and mitochondrial morphology in ART-treated ovarian cancer cells. Erastin, a well-known ferroptosis inducer, was used as a positive control. The results revealed that the increase in ROS and lipid peroxides production induced by ART or Erastin were significantly blocked due to the overexpression of HOXC11 (Fig. 4A, C). Additionally, the decrease of GSH level induced by ART or Erastin was partially recovered due to the overexpression of HOXC11 (Fig. 4B). Moreover, as shown in Fig. 4D, ART obviously induced mitochondrial shrinkage, increased the bilayer membrane density and reduced the number of mitochondrial cristae. An increase in HOXC11 prevented this ferroptosis-like ultrastructure and partially restored mitochondrial morphology. The similar results were also found in the Erastin-treated groups. Therefore, these results suggested that overexpression of HOXC11 attenuated ART-induced ferroptosis in ovarian cancer cells.

Interfering with HOXC11-induced PROM2 recovered the effects of ART on proliferation, apoptosis and migration in ovarian cancer cells

We further investigated whether HOXC11 plays a role through the transcriptional regulation of PROM2. PROM2 knockdown cell lines were generated from HOXC11-overexpressing ES2 and SKOV3 cells via lentivirus infection. The knockdown efficiency was verified

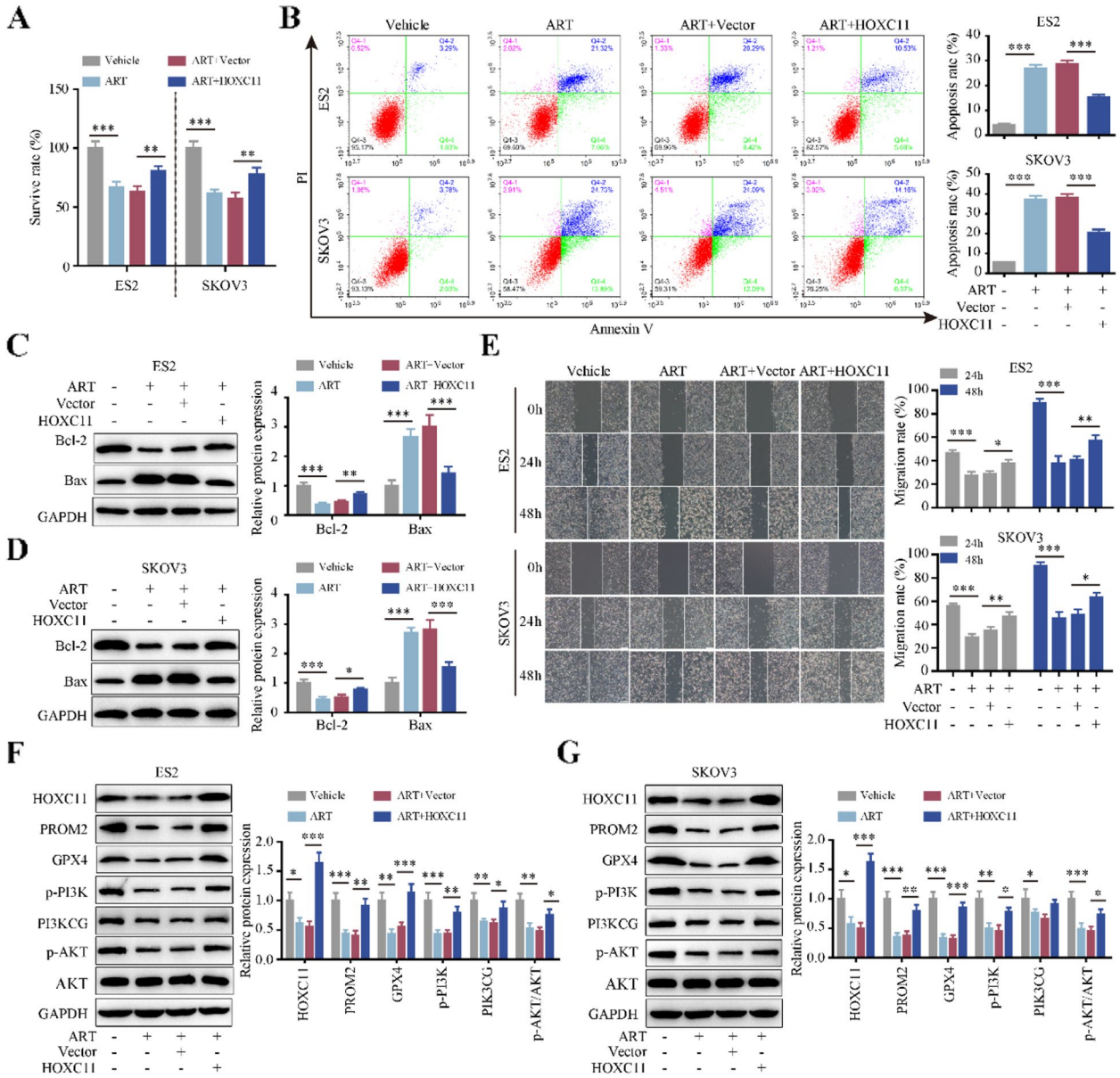

Fig. 3 HOXC11 overexpression suppressed the effects of artesunate (ART)-induced tumor inhibition in ovarian cancer cells by upregulating the PROM2/PI3K/AKT pathway ES2 and SKOV3 cells were treated with DMSO (vehicle) or 40 μM ART for 24 h, and the cells stably overexpressing HOXC11 or a control (vector) were also treated with 40 μM ART for 24 h. **A** Cell viability (% of control) was performed by CCK-8 assay. **B** Cell apoptosis was analyzed by flow cytometry with Annexin V/PI staining. **C**, **D** Western blot analysis of Bcl-2 and Bax in ES2 cells and SKOV3 cells, respectively. GAPDH was used as a loading control. **E** Cell migration ability was determined by a wound scratch assay. Images were taken at 0 h, 24 h and 48 h after scratching (Scale bars = 100 μm). Migration rate (%) = (scratch area at 0 h − scratch area at 24–48 h)/scratch area at 0 h × 100%. **F**, **G** Western blot analysis of HOXC11, PROM2, GPX4, p-PI3K, PI3KCG, p-AKT and AKT in ES2 cells and SKOV3 cells, respectively. GAPDH was used as a loading control. Data were analyzed as the mean ± SD of three independent experiments. *$p < 0.05$. **$p < 0.01$, ***$p < 0.001$

by western blot and sh-PROM2 #1 was chosen for further experiments (Fig. 5A, B). A CCK-8 assay was performed, and the findings indicated that silencing PROM2 recovered the inhibitory effect of ART on proliferation, which was blocked by HOXC11 overexpression (Fig. 5C). In addition, ART-induced apoptosis was restored after interfering PROM2, which was inhibited by HOXC11 overexpression (Fig. 5D). Moreover, silencing PROM2 reversed the effect of HOXC11 on the expression of apoptosis-related proteins by increasing the expression of Bcl-2 and decreasing the expression of Bax (Fig. 5E, F). Additionally, wound healing assays indicated that

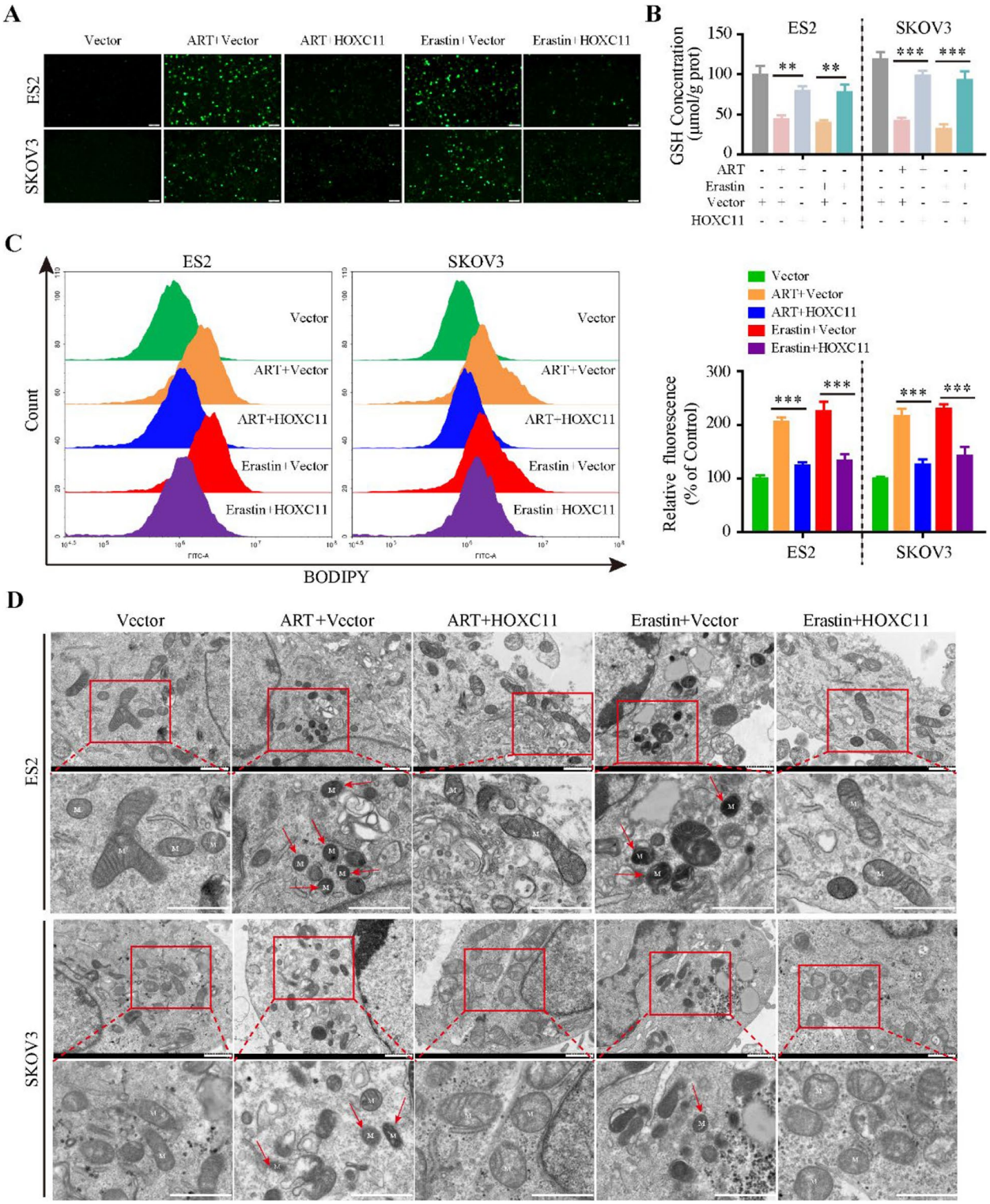

Fig. 4 HOXC11 enhanced artesunate (ART)-induced ferroptosis resistance in ovarian cancer cells ES2 and SKOV3 cells stably overexpressing HOXC11 or control (vector) in the presence of 40 μM ART or 5 μM Erastin for 24 h. **A** Intracellular reactive oxygen species (ROS) levels were measured using DCFH-DA probes using microscope. **B** Intracellular glutathione (GSH) concentrations were determined using a GSH assay kit. **C** Intracellular lipid peroxidation levels were analyzed using BODIPY 581/591 C11 by flow cytometry (left), and the relative fluorescence intensity was calculated (right). **D** Transmission electron microscope (TEM) images of mitochondrial (M) morphology (Scale bars = 1 μm). The red arrows indicated representative ferroptosis-like mitochondria. Data were analyzed as the mean ± SD of three independent experiments. $^{**}p < 0.01$, $^{***}p < 0.001$

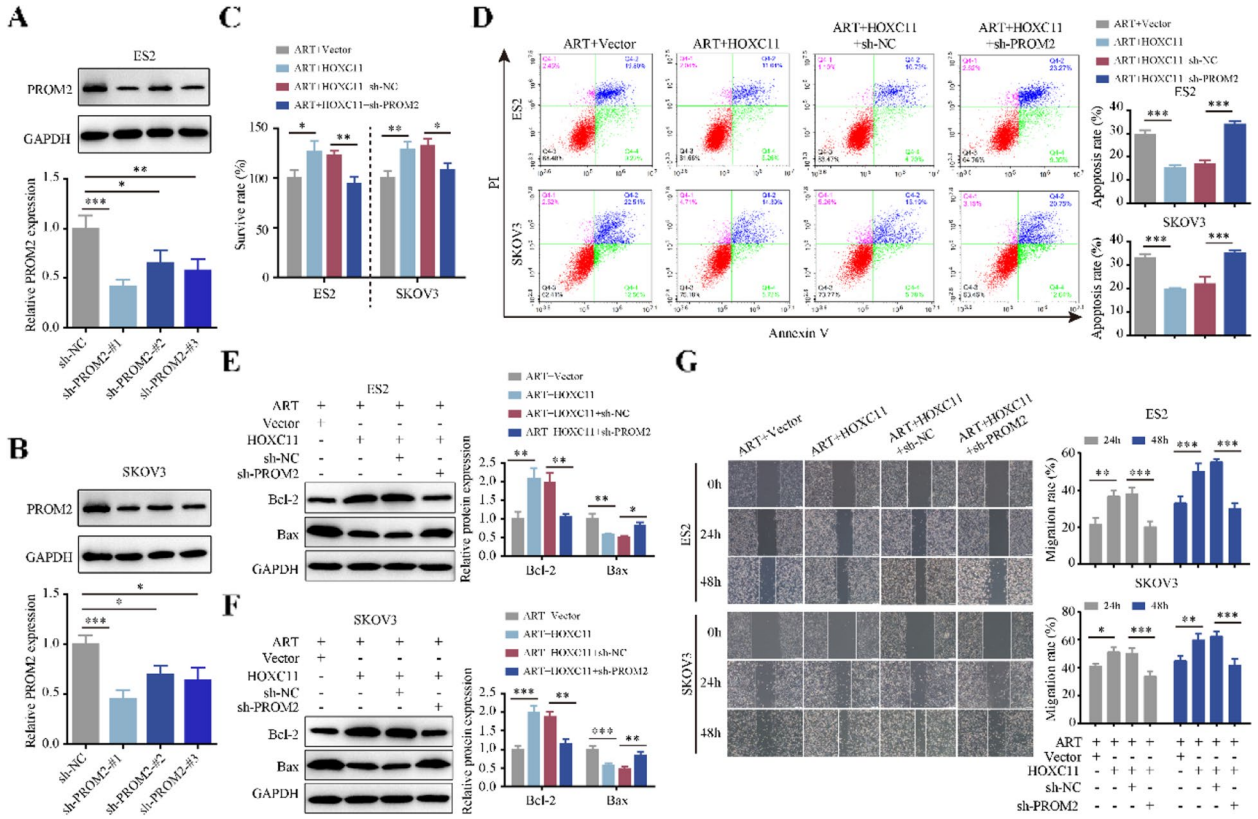

Fig. 5 Interfering HOXC11-induced PROM2 recovered the effects of artesunate (ART) on proliferation, apoptosis and migration in ovarian cancer cells (**A**, **B**) Western blot analysis of PROM2 expression in ES2 cells and SKOV3 cells infected with lentivirus encoding the *PROM2* shRNA (sh-PROM2-#1, sh-PROM2-#2 and sh-PROM2-#3) or scrambled shRNA (sh-NC). GAPDH was used as a loading control. sh-PROM2-#1 was selected for further study. ES2 and SKOV3 cells were infected with lentivirus overexpressing HOXC11 alone or in combination with PROM2 shRNA in the presence of 40 μM ART for 24 h. **C** Cell viability (% of control) was determined by CCK-8 assay in ES2 and SKOV3 cells. **D** Cell apoptosis was analyzed by flow cytometry using Annexin V/PI staining. **E**, **F** Western blot analysis of Bcl-2 and Bax expression in ES2 cells and SKOV3 cells, respectively. GAPDH was used as a loading control. **G** Cell migration ability was determined by wound scratch assay. Images were taken at 0 h, 24 h and 48 h after scratching (Scale bars = 100 μm). Migration rate (%) = (scratch area at 0 h − scratch area at 24–48 h)/scratch area at 0 h × 100%. Data were analyzed as the mean ± SD of three independent experiments. *$p < 0.05$. **$p < 0.01$, ***$p < 0.001$

knockdown of PROM2 reversed cell migration ability, which was caused by overexpression of HOXC11 in ART-treated ES2 and SKOV3 cells (Fig. 5G). These results suggested that silencing PROM2 could reverse the function of HOXC11 overexpression and partially restore ART-induced proliferation, apoptosis and migration in ovarian cancer cells.

Silencing PROM2 attenuated the effects of HOXC11 on ART-induced ferroptosis

Subsequently, we investigated the involvement of PROM2 in HOXC11-related ferroptosis in ES2 and SKOV3 cells treated with ART. As expected, PROM2 interference inhibited the PI3K/AKT and GPX4 levels that were activated by HOXC11 overexpression in ART-treated cells (Fig. 6A, B). Moreover, PROM2 knockdown weakened HOXC11-mediated ferroptosis inhibition, as indicated by the restoration of ROS accumulation and GSH depletion (Fig. 6C, D), along with increased lipid peroxides production (Fig. 6E). Taken together, silencing PROM2 attenuated the effects of HOXC11 overexpression and partially restored ART-induced ferroptosis.

Artesunate induced ferroptosis-mediated tumor inhibition by suppressing the HOXC11/PROM2/PI3K/AKT pathway in vivo

Based on our in vitro findings, we further investigated the mechanisms of ART-induced ferroptosis in a xenograft mouse model. SKOV3 cells were inoculated into BALB/c nude mice and treated with either vehicle control or ART (Fig. 7A). The results showed that the xenografts in the ART-treated group were significantly smaller than those in the vehicle group (Fig. 7B, C, E), with no significant body weight loss in either group of mice during treatment (Fig. 7D). In addition, ART treatment significantly induced ferroptosis in tumor tissues, as indicated

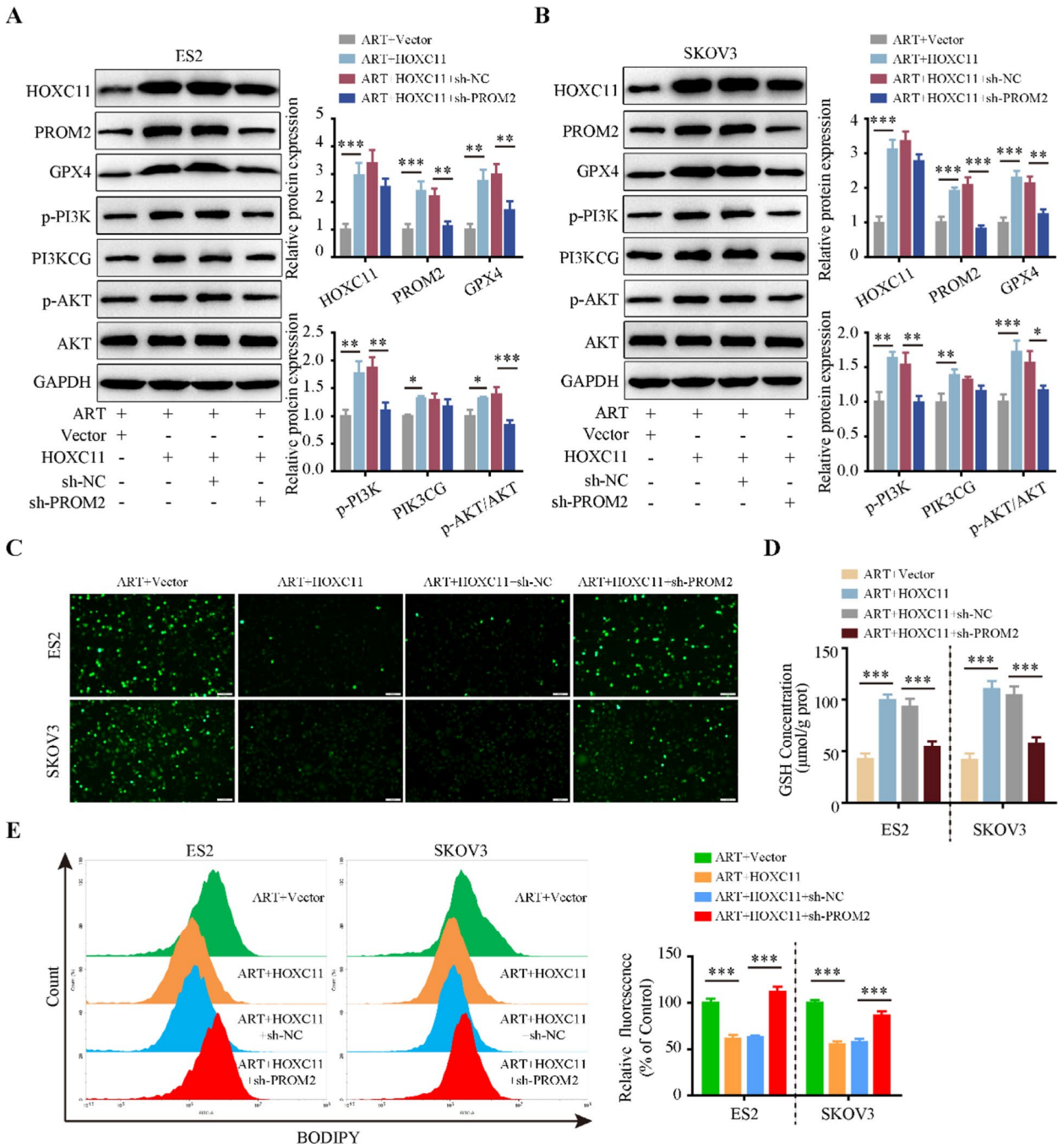

Fig. 6 Silencing PROM2 attenuated the effects of HOXC11 overexpression and partially recovered artesunate (ART)-induced ferroptosis ES2 and SKOV3 cells were infected with lentivirus overexpressing HOXC11 alone or in combination with PROM2 shRNA in the presence of 40 μM ART for 24 h. **A**, **B** Western blot analysis of HOXC11, PROM2, GPX4, p-PI3K, PI3KCG, p-AKT and AKT in ES2 cells and SKOV3 cells, respectively. GAPDH was used as a loading control. **C** Intracellular reactive oxygen species (ROS) levels were measured with DCFH-DA probes using microscope. **D** Intracellular glutathione (GSH) concentrations were determined using a GSH assay kit. **E** Intracellular lipid peroxidation levels were analyzed using BODIPY 581/591 C11 by flow cytometry (left) and the relative fluorescence intensity was calculated (right). Data were analyzed as the mean ± SD of three independent experiments. *$p < 0.05$. **$p < 0.01$, ***$p < 0.001$

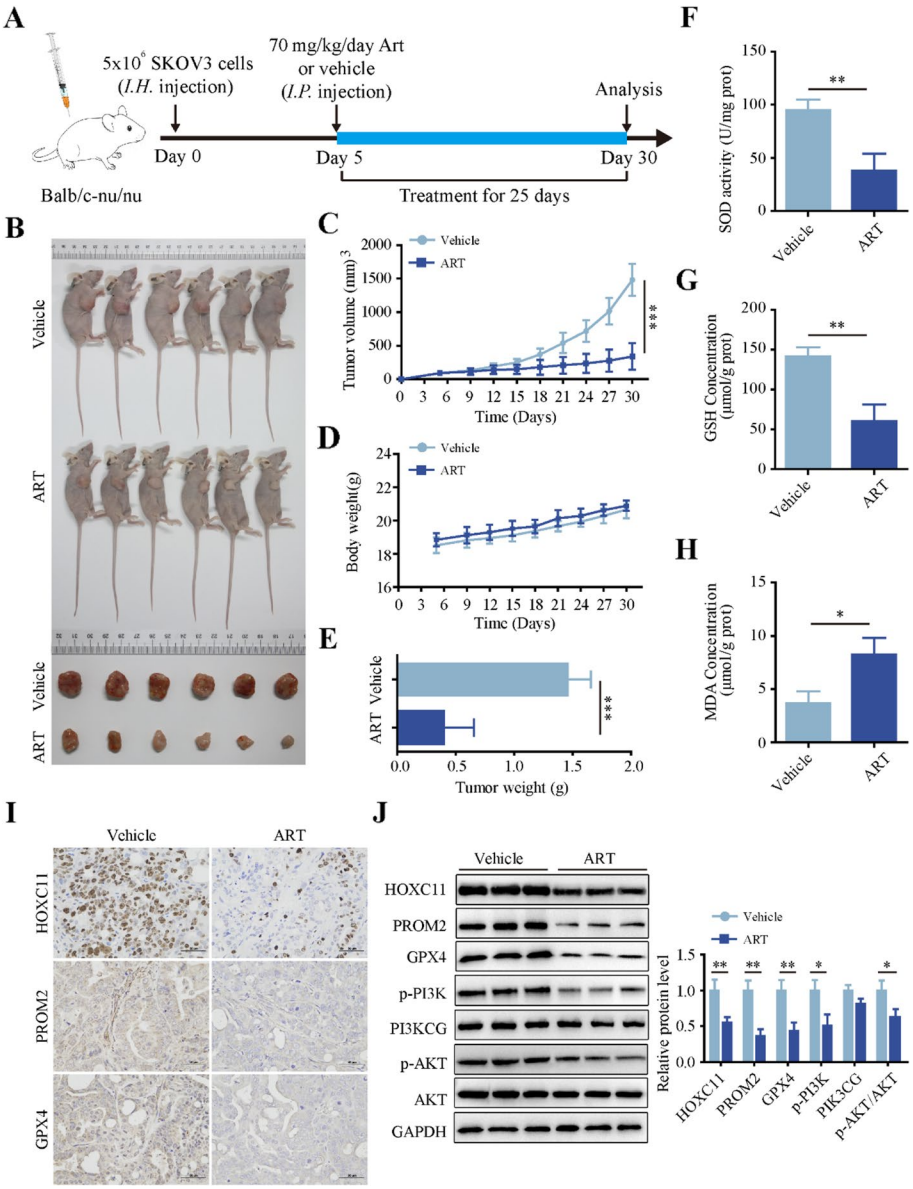

Fig. 7 Artesunate (ART) induced ferroptosis-mediated tumor inhibition by suppressing the HOXC11/PROM2/PI3K/AKT pathway in a SKOV3 xenograft mouse model (**A**) Scheme of the experimental design and timeline for the tumor model. SKOV3 cells (5×10^6 cells for each mouse) were inoculated into BALB/c-nude mice subcutaneously. Tumor-bearing mice were treated with vehicle (5% DMSO) or ART at 70 mg/kg daily for 25 days ($n = 6$ for each group). Body weights and tumor volumes were monitored every three days. **B** Images of xenograft nude mice and tumor mass. **C** Curve of tumor volume. **D** Curve of body weight. **E** Tumor weight. The superoxide dismutase (SOD) activity (**F**), glutathione (GSH) levels (**G**) and malondialdehyde (MDA) levels (**H**) were measured in the tumor tissue of nude mice. **I** IHC staining was performed to detect the expression of HOXC11, PROM2 and GPX4 in the tumor tissues of xenografted mice. **J** Western blot analysis of HOXC11, PROM2, GPX4, p-PI3K, PI3KCG, p-AKT and AKT in tumor tissue samples obtained from xenograft mice treated with vehicle or ART. GAPDH was used as a loading control. Data were analyzed as the mean ± SD of three independent experiments. $^*p < 0.05$. $^{**}p < 0.01$, $^{***}p < 0.001$

by decreased SOD activity and GSH levels (Fig. 7F, G), reduced GPX4 expression (Fig. 7I, J), and increased MDA levels (Fig. 7H). Furthermore, we investigated the expression of HOXC11, PROM2 and PI3K/AKT signaling. The IHC results suggested that ART decreased the expression of HOXC11 and PROM2 (Fig. 7I). Finally, western blot analysis further revealed decreased HOXC11, PROM2, p-PI3K, PIK3CG and p-AKT/AKT expression in the ART-treated xenografts (Fig. 7J). Overall, the results indicated that the mechanism of ART-induced ferroptosis in the xenograft model involved the inhibition of the HOXC11/PROM2/PI3K/AKT pathway.

Discussion

Ovarian cancer is one of the most common gynecologic tumors in women and is a leading cause of mortality [1]. In recent years, effective therapies have been developed to improve survival rates. However, due to chemoresistance and high rates of recurrence the treatment of ovarian cancer remains a significant challenge [2]. An increasing number of studies have shown that ferroptosis, a form of regulated cell death, plays a critical role in cancers development and progression, making it a potential strategy for cancer treatment. For example, inhibition of GPX4 disrupts intracellular lipid peroxide reducibility and iron homeostasis, which contributes to ferroptosis and has anticancer effects [27]. Inhibition of poly ADP-ribose polymerase (PARP) downregulates the biosynthesis of GSH and promotes lipid peroxidation, leading to ferroptosis and preventing BRCA-proficient ovarian cancer [28]. Although cancer cells are always in a state of excessive oxidative stress, they seldom undergo ferroptosis, which is mainly due to their antioxidant system [29, 30]. Therefore, further investigation into the mechanisms that regulate ferroptosis in cancer cells is important for developing novel therapeutic strategies [4].

ART is a derivative of artemisinin and it has been reported to be involved in ferroptosis in several cancer cells in recent years [23–25]. However, there are few studies on ART in ovarian cancer, and the mechanism of ART-induced ferroptosis needs to be further investigated. In this study, we performed RNA-seq using ART-treated ES2 cells to investigate the mechanism by which ART regulates ferroptosis in ovarian cancer cells. We identified nine candidate genes by intersecting ferroptosis suppressor genes from the FerrDb database with downregulated DEGs induced by ART. Among them, PROM2 attracted our attention due to its reported involvement in ferroptosis, although it has not been studied in ovarian cancer.

In further studies, HOXC11 was predicted to be a potential transcription factor regulating PROM2 expression. This prediction was verified through dual-luciferase reporter assay and EMSA. HOXC11 is usually upregulated in most types of solid tumors and is associated with poor prognosis [15–17]. However, its role in ferroptosis has not been reported previously. Our study is the first one to demonstrate that HOXC11 is involved in regulating ART-induced ferroptosis in ovarian cancer cells. We found that HOXC11 overexpression inhibited ART-induced antitumor activity in ovarian cancer cells, as evidenced by the suppression of proliferation, migration, apoptosis and the expression of apoptosis-associated proteins. Moreover, HOXC11 plays an important regulatory role in ART-induced ferroptosis. Specifically, ART treatment inhibited GPX4 expression, whereas HOXC11 overexpression restored GPX4 levels. GPX4, a GSH-dependent enzyme, plays a vital role in ferroptosis through preventing lipid hydroperoxide formation [31]. Previous studies have shown that decreasing GPX4 sensitizes UMRC6 cancer cells to ferroptosis [32]. However, increased expression of GPX4 caused by abnormal activation of Wnt/beta-catenin signaling leads to ferroptosis resistance in gastric cancer [33]. In addition, GSH, a key cofactor for GPX4, is a strong scavenger of lipid peroxides and plays a crucial role in ferroptosis [34]. A previous study showed that ART induces a potent generation of ROS, contributing to the suppression of ovarian cancer cell proliferation and tumor growth *in* an animal model [25]. In this study, we also found that a decrease in GSH levels and an increase in ROS and lipid peroxides production were induced by ART, while these effects were significantly blocked by HOXC11 overexpression. Furthermore, mitochondrial morphological abnormality is one of the characteristics of ferroptosis [6, 35]. After ART treatment, mitochondrial shrinkage, increased bilayer membrane density and reduced mitochondrial cristae were clearly observed. However, HOXC11 overexpression mitigated these changes and partially restored mitochondrial morphology. These results suggested that ART-mediated ferroptosis is at least partially regulated by HOXC11 expression in ovarian cancer cells.

PROM2 is a transmembrane glycoprotein that is upregulated in many cancers [18]. PROM2-activated iron export promotes tumorigenesis and ferroptosis resistance in bladder cancer and breast cancer [36, 37]. This study investigated whether HOXC11 is involved in ART-induced ferroptosis by transcriptionally regulating PROM2. The results indicated that silencing PROM2 could weaken the function of overexpressed HOXC11 and partially restored the effects of ART on proliferation, apoptosis and migration in ovarian cancer cells. In addition, the characteristics of ferroptosis, such as decreased GPX4 levels, ROS accumulation, increased lipid peroxides production and GSH depletion, were restored after silencing PROM2. Taken together, our findings suggested that PROM2 is regulated by HOXC11 and that targeting PROM2 may reverse HOXC11-mediated suppression of ART-induced ferroptosis. These results are in accordance with the opinion that targeting PROM2 may be a potential cancer therapy by inducing ferroptosis [38]. PROM2 has also been reported to promote gemcitabine resistance [39] and decrease cisplatin sensitivity [40]; therefore, the combination of ART with other chemotherapeutic drugs may be a good strategy for preventing PROM2-mediated drug resistance in cancer cells.

Our data further revealed that downregulated DEGs in ART-treated cells were significantly enriched in the PI3K-AKT signaling pathway. Recent studies have also

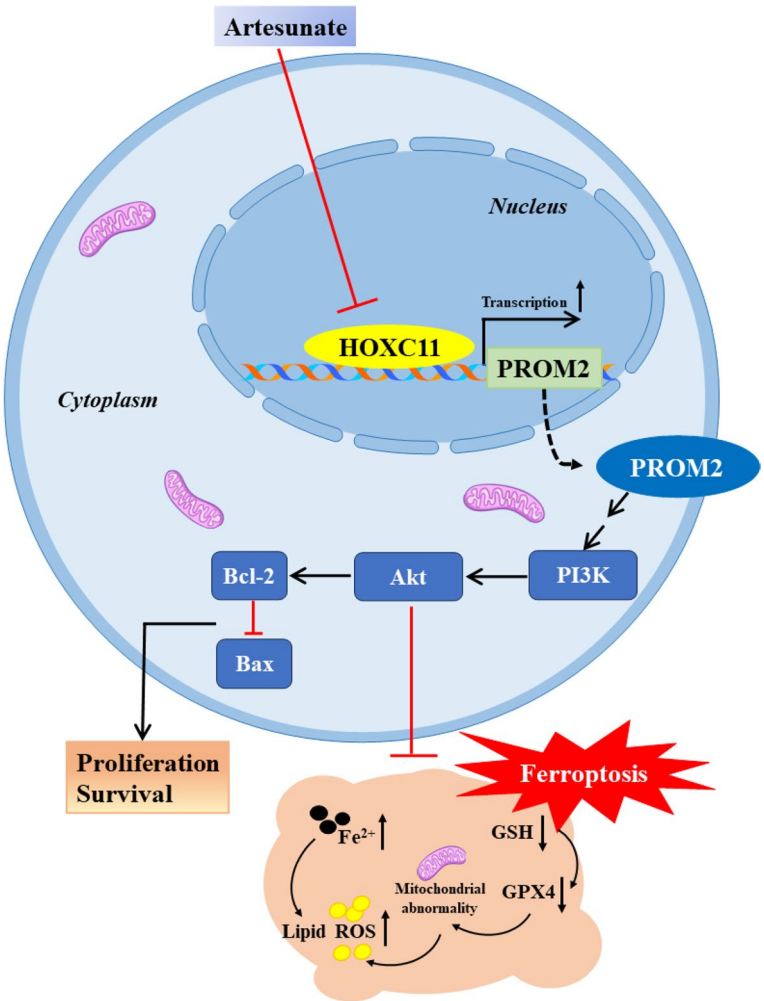

Fig. 8 The mechanism of ART induced ferroptosis by suppressing the HOXC11/PROM2/PI3K/AKT pathway in ovarian cancer ART induces ferroptosis through promoting lipid peroxidation, accumulating reactive oxygen species (ROS) and depleting glutathione (GSH), while also promoting Bcl-2/Bax dependent apoptosis in ovarian cancer. Mechanistically, ART inhibits the expression of HOXC11, a transcription factor that regulates the PROM2/PI3K/AKT pathway by binding to the PROM2 promoter directly

demonstrated the involvement of PI3K/AKT signaling in regulating ferroptosis. For example, lapatinib promotes mitochondrial dysfunction to increase ferroptosis and oxidative stress via inhibition of the PI3K/AKT signaling pathway in doxorubicin-induced cardiomyocytes [41]. Oncogenic activation of PI3K-AKT-mTOR signaling inhibits ferroptosis through sterol regulatory element-binding protein 1 (SREBP1) mediated lipogenesis [42]. In addition, it has been reported that PROM2 promotes cancer progression by regulating the PI3K/AKT pathway [39, 43]. Therefore, we hypothesized that HOXC11 might mediate ferroptosis by regulating the PROM2/PI3K/AKT pathway. As expected, overexpression of HOXC11 attenuated the inhibitory effects of ART on the PROM2/PI3K/AKT signaling, while PROM2 silencing blocked the function of HOXC11 and restored the regulatory effect of ART on PI3K/AKT signaling. We further confirmed that ART-induced tumor inhibition via ferroptosis through inhibiting the HOXC11/PROM2/PI3K/AKT pathway in a SKOV3 xenograft mouse model.

Currently, chemotherapy regimens for ovarian cancer mainly include platinum-based and paclitaxel drugs. However, the prognosis of patients with advanced-stage disease remains poor [4]. It has been proposed that ovarian cancer cells exhibit increased iron uptake and decreased iron efflux, which may increase their sensitivity to ferroptosis inducers [44]. In the present study, we demonstrated that ART could induce ferroptosis in ovarian cancer cells. Previous studies have also shown that ART selectively kills tumor cells with minimal side effects

on normal cells [45]. Moreover, our findings revealed that the HOXC11 /PROM2 axis plays a crucial role in regulating ART-induced ferroptosis. Our results suggested that targeting the HOXC11/PROM2 axis could be a promising therapeutic strategy for ovarian cancer.

Conclusion

In summary, our study demonstrated for the first time that ART-induces inhibition of HOXC11 triggers ferroptosis and suppresses ovarian cancer progression both in vitro and in vivo. Mechanistically, HOXC11 regulates PROM2 expression by binding to its promoter directly. Overexpressing HOXC11 reversed the function of ART through transcriptional regulation of the PROM2/PI3K/AKT pathway, while silencing PROM2 in HOXC11-overexpressing cells restores ART-induced ferroptosis (Fig. 8). Our results suggest that ART is a prospective antitumor drug and the HOXC11/PROM2 axis represents a potential therapeutic target for ovarian cancer.

Supplementary Information

The online version contains supplementary material available at https://doi.org/10.1186/s12957-024-03544-w.

Supplementary Material 1.

Supplementary Material 2.

Disclosure statement

The authors declare that they have no conflicts of interest.

Authors' contributions

All the authors contributed to the study conception and design. Material preparation, data collection and analysis were performed by J L, L F, Y Y, T H, X Z, B S, X Y, and K L. The first draft of the manuscript was written by J L and L F. The final manuscript was edited by X Y and K L. All authors commented on previous versions of the manuscript. All the authors have read and approved the final manuscript.

Funding

This work was supported by the Nanchong Science and Technology Program. The grant numbers are 22SXQT0344 and 22SXQT0134; University Level Research and Development Fund Project of North Sichuan Medical College, the grant numbers are CBY23-ZDA12 and CBY23-QNA11.

Availability of data and materials

No datasets were generated or analysed during the current study.

Declarations

Ethics approval and consent to participate

All animal experiments were performed under the institutional guidelines and were approved by the Ethics Committees of North Sichuan Medical College (NSMC2023 (114)).

Competing interests

The authors declare no competing interests.

Author details

[1]Department of Obstetrics and Gynecology, the First Affiliated Hospital of Soochow University, Suzhou 215006, PR China. [2]Department of Obstetrics and Gynecology, Nanchong Central Hospital, The Second Clinical Medical College of North Sichuan Medical College, Nanchong, Sichuan, PR China. [3]Institute of Tissue Engineering and Stem Cell, Nanchong Central Hospital, The Second Clinical Medical College of North Sichuan Medical College, Nanchong, Sichuan, PR China.

Received: 14 May 2024 Accepted: 1 October 2024
Published online: 08 October 2024

References

1. Havasi A, Cainap SS, Havasi AT, Cainap C. Ovarian cancer-insights into platinum resistance and overcoming it. Med (Kaunas). 2023;59(3): 544. https://doi.org/10.3390/medicina59030544.
2. Zhang R, Siu MKY, Ngan HYS, Chan KKL. Molecular biomarkers for the early detection of ovarian cancer. Int J Mol Sci. 2022;23(19): 12041. https://doi.org/10.3390/ijms231912041.
3. Sung H, Ferlay J, Siegel RL, Laversanne M, Soerjomataram I, Jemal A, et al. Global cancer statistics 2020: globocan estimates of incidence and mortality worldwide for 36 cancers in 185 countries. CA Cancer J Clin. 2020;71(3):209–49. https://doi.org/10.3322/caac.21660.
4. Zhang C, Liu N. Ferroptosis, necroptosis, and pyroptosis in the occurrence and development of ovarian cancer. Front Immunol. 2022;13: 920059. https://doi.org/10.3389/fimmu.2022.920059.
5. Dixon SJ, Lemberg KM, Lamprecht MR, Skouta R, Zaitsev EM, Gleason CE, et al. Ferroptosis: an iron-dependent form of nonapoptotic cell death. Cell. 2012;149(5):1060–72. https://doi.org/10.1016/j.cell.2012.03.042.
6. Li J, Cao F, Yin HL, Huang ZJ, Lin ZT, Mao N, et al. Ferroptosis: past, present and future. Cell Death Dis. 2020;11(2):88. https://doi.org/10.1038/s41419-020-2298-2.
7. Moujalled D, Southon AG, Saleh E, Brinkmann K, Ke F, Iliopoulos M, et al. BH3 mimetic drugs cooperate with Temozolomide, JQ1 and inducers of ferroptosis in killing glioblastoma multiforme cells. Cell Death Differ. 2022;29(7):1335–48. https://doi.org/10.1038/s41418-022-00977-2.
8. Chen Y, Li L, Lan J, Cui Y, Rao X, Zhao J, et al. CRISPR screens uncover protective effect of PSTK as a regulator of chemotherapy-induced ferroptosis in hepatocellular carcinoma. Mol Cancer. 2022;21:11. https://doi.org/10.1186/s12943-021-01466-9.
9. Liu S, Zhang HL, Li J, Ye ZP, Du T, Li LC, et al. Tubastatin A potently inhibits GPX4 activity to potentiate cancer radiotherapy through boosting ferroptosis. Redox Biol. 2023;62: 102677. https://doi.org/10.1016/j.redox.2023.102677.
10. Zhou C, Yu T, Zhu R, Lu J, Ouyang X, Zhang Z, et al. Timosaponin AIII promotes non-small-cell lung cancer ferroptosis through targeting and facilitating HSP90 mediated GPX4 ubiquitination and degradation. Int J Biol Sci. 2023;19(5):1471–89. https://doi.org/10.7150/ijbs.77979.
11. Zheng X, Liu J, Hu W, Jiang B, Zhou X, Zhang M, et al. Curcumin induces autophagy-mediated ferroptosis by targeting the PI3K/AKT/mTOR signaling pathway in gastric cancer. Turk J Gastroenterol. 2024;35(8):625–33. https://doi.org/10.5152/tjg.2024.23526.
12. Li J, Jiang JL, Chen YM, Lu WQ. KLF2 inhibits colorectal cancer progression and metastasis by inducing ferroptosis via the PI3K/AKT signaling pathway. J Pathol Clin Res. 2023;9(5):423–35. https://doi.org/10.1002/cjp2.325.
13. Tang S, Shen Y, Wei X, Shen Z, Lu W, Xu J. Olaparib synergizes with arsenic trioxide by promoting apoptosis and ferroptosis in platinum-resistant ovarian cancer. Cell Death Dis. 2022;13(9):826. https://doi.org/10.1038/s41419-022-05257-y.
14. Wang CK, Chen TJ, Tan GYT, Chang FP, Sridharan S, Yu CA, et al. MEX3A mediates p53 degradation to suppress ferroptosis and facilitate ovarian cancer tumorigenesis. Cancer Res. 2023;83(2):251–63. https://doi.org/10.1158/0008-5472.CAN-22-1159.
15. Peng X, Liu X, Hu W, Zhou Y, Ouyang L, Peng X, et al. HOXC11 drives lung adenocarcinoma progression through transcriptional regulation of SPHK1. Cell Death Dis. 2023;14(2):153. https://doi.org/10.1038/s41419-023-05673-8.

16. Liu L, Jia S, Jin X, Zhu S, Zhang S. HOXC11 expression is associated with the progression of colon adenocarcinoma and is a prognostic biomarker. DNA Cell Biol. 2021;40:1158–66.
17. Peng X, Sun J, Long Y, Xiao D, Zhou J, Tao Y, et al. The significance of HOXC11 and LSH in survival prediction in gastric adenocarcinoma. Onco Targets Ther. 2021;14:1517–29.
18. Saha SK, Islam SMR, Kwak KS, Rahman MS, Cho SG. PROM1 and PROM2 expression differentially modulates clinical prognosis of cancer: a multiomics analysis. Cancer Gene Ther. 2020;27:147–67. https://doi.org/10.1038/s41417-019-0109-7.
19. An J, Shi J, Yang C, Luo J, Li Y, Ren J, et al. Regulation of tumorigenesis and ferroptosis in non-small cell lung cancer by a novel BBOX1-AS1/miR-326/PROM2 axis. Mol Cell Biochem. 2023. https://doi.org/10.1007/s11010-023-04837-6.
20. Brown CW, Chhoy P, Mukhopadhyay D, Karner ER, Mercurio AM. Targeting prominin2 transcription to overcome ferroptosis resistance in cancer. EMBO Mol Med. 2021;13(8): e13792. https://doi.org/10.15252/emmm.202013792.
21. Klayman DL. Qinghaosu (artemisinin): an antimalarial drug from China. Science. 1985;228(4703):1049–55. https://doi.org/10.1126/science.3887571. PMID: 3887571.
22. Kiani BH, Kayani WK, Khayam AU, Dilshad E, Ismail H, Mirza B. Artemisinin and its derivatives: a promising cancer therapy. Mol Biol Rep. 2020;47(8):6321–36. https://doi.org/10.1007/s11033-020-05669-z.
23. Eling N, Reuter L, Hazin J, Hamacher-Brady A, Brady NR. Identification of artesunate as a specific activator of ferroptosis in pancreatic cancer cells. Oncoscience. 2015;2(5):517–32. https://doi.org/10.18632/oncoscience.160.
24. Ooko E, Saeed ME, Kadioglu O, Sarvi S, Colak M, Elmasaoudi K, et al. Artemisinin derivatives induce iron-dependent cell death (ferroptosis) in tumor cells. Phytomedicine. 2015;22(11):1045–54. https://doi.org/10.1016/j.phymed.2015.08.002.
25. Greenshields AL, Shepherd TG, Hoskin DW. Contribution of reactive oxygen species to ovarian cancer cell growth arrest and killing by the anti-malarial drug artesunate. Mol Carcinog. 2017;56(1):75–93. https://doi.org/10.1002/mc.22474.
26. Ding N, He H, Yuan Y, Lu Q, Hu H, Liu K, et al. Artesunate induces ferroptosis via modulation of Wnt/β-catenin signaling pathway in ovarian cancer cells. Prog Obstet Gynecol. 2023;32(7):26–31. https://doi.org/10.13283/j.cnki.xdfckjz.2023.07.033.
27. Li D, Zhang M, Chao H. Significance of glutathione peroxidase 4 and intracellular iron level in ovarian cancer cells-utilization of ferroptosis mechanism. Inflamm Res. 2021;70(10–12):1177–89. https://doi.org/10.1007/s00011-021-01495-6.
28. Hong T, Lei G, Chen X, Li H, Zhang X, Wu N, et al. PARP inhibition promotes ferroptosis via repressing SLC7A11 and synergizes with ferroptosis inducers in BRCA-proficient ovarian cancer. Redox Biol. 2021;42: 101928. https://doi.org/10.1016/j.redox.2021.101928.
29. Lei G, Zhuang L, Gan B. Targeting ferroptosis as a vulnerability in cancer. Nat Rev Cancer. 2022;22:381–96. https://doi.org/10.1038/s41568-022-00459-0.
30. Zhang C, Liu X, Jin S, Chen Y, Guo R. Ferroptosis in cancer therapy: a novel approach to reversing drug resistance. Mol Cancer. 2022;21:47. https://doi.org/10.1186/s12943-022-01530-y.
31. Yang WS, SriRamaratnam R, Welsch ME, Shimada K, Skouta R, Viswanathan VS, et al. Regulation of ferroptotic cancer cell death by GPX4. Cell. 2014;156(1–2):317–31. https://doi.org/10.1016/j.cell.2013.12.010.
32. Zhang Y, Swanda RV, Nie L, Liu X, Wang C, Lee H, et al. mTORC1 couples cyst(e)ine availability with GPX4 protein synthesis and ferroptosis regulation. Nat Commun. 2021;12(1):1589. https://doi.org/10.1038/s41467-021-21841-w.
33. Wang Y, Zheng L, Shang W, Yang Z, Li T, Liu F, et al. Wnt/beta-catenin signaling confers ferroptosis resistance by targeting GPX4 in gastric cancer. Cell Death Differ. 2022;29(11):2190–202. https://doi.org/10.1038/s41418-022-01008-w.
34. Cao JY, Poddar A, Magtanong L, Lumb JH, Mileur TR, Reid MA, et al. A genome-wide haploid genetic screen identifies regulators of glutathione abundance and ferroptosis sensitivity. Cell Rep. 2019;26(6):1544-e15568. https://doi.org/10.1016/j.celrep.2019.01.043.
35. Xu T, Liu Y, Zhao Z, Liu J, Chai J, Yang Y, et al. Ferroptosis in cancer stem cells. Pathol Res Pract. 2023;245: 154492. https://doi.org/10.1016/j.prp.2023.154492.
36. Brown CW, Amante JJ, Chhoy P, Elaimy AL, Liu H, Zhu LJ, et al. Prominin2 drives ferroptosis resistance by stimulating iron export. Dev Cell. 2019;51(5):575-e5864. https://doi.org/10.1016/j.devcel.2019.10.007.
37. Luo W, Wang J, Xu W, Ma C, Wan F, Huang Y, et al. LncRNA RP11-89 facilitates tumorigenesis and ferroptosis resistance through PROM2-activated iron export by sponging mir-129-5p in bladder cancer. Cell Death Dis. 2021;12(11):1043. https://doi.org/10.1038/s41419-021-04296-1.
38. Brown CW, Chhoy P, Mukhopadhyay D, Karner ER, Mercurio AM. Targeting prominin2 transcription to overcome ferroptosis resistance in cancer. EMBO Mol Med. 2021;13(8): e13792.
39. Li W, Zhu Y, Zhang K, Yu X, Lin H, Wu W, et al. PROM2 promotes gemcitabine chemoresistance via activating the akt signaling pathway in pancreatic cancer. Exp Mol Med. 2020;52(3):409–22. https://doi.org/10.1038/s12276-020-0390-4.
40. Tang J, Shu D, Fang Z, Yang G. Prominin 2 decreases cisplatin sensitivity in non-small cell lung cancer and is modulated by CTCC binding factor. Radiol Oncol. 2023;57(3):325–36. https://doi.org/10.2478/raon-2023-0033.
41. Sun L, Wang H, Xu D, Yu S, Zhang L, Li X. Lapatinib induces mitochondrial dysfunction to enhance oxidative stress and ferroptosis in doxorubicin-induced cardiomyocytes via inhibition of PI3K/AKT signaling pathway. Bioengineered. 2022;13(1):48–60. https://doi.org/10.1080/21655979.2021.2004980.
42. Yi J, Zhu J, Wu J, Thompson CB, Jiang X. Oncogenic activation of PI3K-AKT-mTOR signaling suppresses ferroptosis via SREBP-mediated lipogenesis. Proc Natl Acad Sci. 2020;117(49):31189–97. https://doi.org/10.1073/pnas.2017152117.
43. Jiang J, Zhang C, Wang J, Zhu Y, Wang X, Mao P. Knockdown of PROM2 enhances Paclitaxel Sensitivity in Endometrial Cancer cells by regulating the AKT/FOXO1 pathway. Anticancer Agents Med Chem. 2023;23(19):2127–34. https://doi.org/10.2174/1871520623666230905104555.
44. Basuli D, Tesfay L, Deng Z, Paul B, Yamamoto Y, Ning G, et al. Iron addiction: a novel therapeutic target in ovarian cancer. Oncogene. 2017;36(29):4089–99. https://doi.org/10.1038/onc.2017.11.
45. Lai H, Sasaki T, Singh NP, Messay A. Effects of artemisinin-tagged holotransferrin on cancer cells. Life Sci. 2005;76(11):1267–79. https://doi.org/10.1016/j.lfs.2004.08.020.

Publisher's Note